

# Neutron stars in Einstein-aether theory

Christopher Eling<sup>\*1</sup>, Ted Jacobson<sup>\*2</sup>, and M. Coleman Miller<sup>†3</sup>

*\*Department of Physics  
University of Maryland  
College Park, MD 20742-4111, USA*

*†Department of Astronomy  
University of Maryland  
College Park, MD 20742-4111, USA*

## Abstract

As current and future experiments probe strong gravitational regimes around neutron stars and black holes, it is desirable to have theoretically sound alternatives to General Relativity against which to test observations. Here we study the consequences of one such generalization, Einstein-aether theory, for the properties of non-rotating neutron stars. This theory has a parameter range that satisfies all current weak-field tests. We find that within this range it leads to lower maximum neutron star masses, as well as larger surface redshifts at a particular mass, for a given nuclear equation of state. For non-rotating black holes and neutron stars, the innermost stable circular orbit is only slightly modified in this theory.

---

<sup>1</sup>E-mail: cteling@physics.umd.edu

<sup>2</sup>E-mail: jacobson@umd.edu

<sup>3</sup>E-mail: miller@astro.umd.edu

# 1 Introduction

General Relativity (GR) has passed every test so far, from solar system dynamics and light bending to precision measurements of the orbits of binary pulsars [1]. Nonetheless, tests in strong gravity remain elusive, largely because phenomena in strong gravity involve other uncertain physics as well. For example, spectral profiles of Fe K $\alpha$  fluorescence lines in active galactic nuclei and stellar-mass black holes [2, 3, 4, 5, 6] are consistent with the expectations of gas streamlines near rapidly rotating black holes. However, precision tests are not yet possible because of unknowns about the emission profile and other complications.

More robust tests are on the horizon. Larger-area X-ray detectors such as *Constellation-X* [7] may be able to track the motion of individual emitting elements in a disk, hence mapping out the spacetime near a rotating black hole. Even more robustness is likely to come from detections of gravitational waves from double black hole mergers of various masses and mass ratios seen with ground-based interferometers such as LIGO [8], VIRGO [9], GEO-600 [10], and TAMA [11] and later with space-based instruments such as LISA [12]. A third source of strong field tests could exploit neutron star masses and surface redshifts. It is that sort of system that is the subject of this paper.

It is therefore desirable for current and future data to have theoretically sound—and preferably well-motivated—alternatives to or generalizations of GR. The simplest alternatives that have been considered are various scalar-tensor theories. In the case of the well-known Jordan-Brans-Dicke theory it has been shown [13] that the predictions of the theory in both the weak and strong field regimes deviate from GR by a parameter that is tightly constrained by post-Newtonian Solar System experiments. Thus, the properties of compact objects such as neutron stars in Jordan-Brans-Dicke theories that pass these weak field tests must be very close to those found in GR. However, Damour and Esposito-Farese [14] found a wide class of other scalar-tensor theories exhibiting “spontaneous scalarization,” where weak field constraints are met, but compact objects have significant deviations from GR in the strong field regime. Recently, [15] studied the properties of non-rotating neutron stars in these theories, finding larger stellar masses than in GR and larger surface redshifts for a given equation of state. These results were then used to put an observational constraint on one of the parameters of the model.

Over the past several years, a number of further alternatives to GR have been proposed in the context of incorporating Lorentz violation (LV) into gravity; see for example Refs. [16, 17, 18, 19, 20, 21, 22, 23] and references therein. These theories can be thought of as low energy effective field theory descriptions of local Lorentz violation (LV) possibly arising from quantum gravitational physics at energies near the Planck scale. In this paper we study one of these models, “Einstein-aether” theory (or “ae-theory” for short) [24], in which a dynamical unit timelike vector field  $u^a$  is coupled to gravity. The LV here is a sort of spontaneous symmetry breaking. The action is Lorentz invariant, but in any solution defines the 4-velocity of a local “preferred” frame at each spacetime point, which breaks local boost symmetry.

The general ae-theory dynamics is dependent on four dimensionless coupling parameters. Weak field constraints on ae-theory can all be met by restricting these parameters to a subset of the four dimensional parameter space that is very narrow compared to unity in all but one dimension. The nature of these constraints is summarized in the following section. They are derived in the weak field regime, except for strongly self-gravitating neutron star binaries. It is therefore interesting to ask what are the deviations from general relativity in the strong field regime, and to compare that behavior with observations of astrophysical systems.

The main objective of this paper is to study the properties of non-rotating neutron stars in ae-theory. The stellar solutions depend on only one combination of the theory’s coupling parameters. We consider six candidate equations of state, three with purely nucleonic degrees of freedom and different hardness, and three involving quark matter with different bag constants. By numerical solution of the field equations interior to the star we obtain the maximum mass, relation between mass and radius, and surface redshifts, all as a function of the coupling parameter.

It turns out that the maximum neutron star mass is less than in the case of GR, and is smaller for larger values of the coupling parameter. Thus, once the equation of state becomes known well enough, it will be possible to place an upper bound on the coupling parameter by observations of neutron star masses. Nonstandard relations between mass and surface redshift also occur, providing another possibility for interesting phenomenology and constraining the coupling parameter.

We also examine the location of the innermost stable circular orbit (ISCO) as a function of mass, to determine whether that might provide further useful observables distinguishing GR and ae-theory. We find however that the ISCO

is nearly unchanged for reasonable coupling parameters and non-spinning objects.

The structure of this paper is as follows. In Section II we first review the basics of Einstein-aether theory and summarize the current constraints on theory. In Section III the equations of structure for fluid stars in ae-theory are presented, together with the form of the analytic exterior solution to which the interior must be matched. Using the exterior solution, expressions are obtained for the surface redshift and ISCO radius that can be employed with the numerical solutions to obtain the observable quantities. We present the numerical results in Section IV, together with the constraints on the coupling parameter that can be obtained with these results. In Section V we conclude with a brief discussion of prospects for further constraints from more precise neutron star measurements and rotating black hole solutions.

## 2 Einstein-aether theory

The action for Einstein-aether theory is the most general generally covariant functional of the spacetime metric  $g_{ab}$  and aether field  $u^a$  involving no more than two derivatives (not including total derivatives),

$$S = \frac{1}{16\pi G} \int \sqrt{-g} (L_{\text{ae}} + L_{\text{matter}}) d^4x \quad (1)$$

where

$$L_{\text{ae}} = -R - K^{abmn} \nabla_a u_m \nabla_b u_n - \lambda(g^{ab} u_a u_b - 1) \quad (2)$$

and  $L_{\text{matter}}$  denoted the matter lagrangian. Here  $R$  is the Ricci scalar,  $K_{mn}^{ab}$  is defined as

$$K_{mn}^{ab} = c_1 g^{ab} g_{mn} + c_2 \delta_m^a \delta_n^b + c_3 \delta_n^a \delta_m^b + c_4 u^a u^b g_{mn} \quad (3)$$

where the  $c_i$  are dimensionless coupling constants, and  $\lambda$  is a Lagrange multiplier enforcing the unit timelike constraint on the aether. The convention used here for metric signature is  $(+---)$  and the units are chosen so that the speed of light defined by the metric  $g_{ab}$  is unity. Note that since the covariant derivative operator  $\nabla_a$  involves derivatives of the metric through the connection components, and since the unit vector is nowhere vanishing, the terms quadratic in  $\nabla u$  also modify the kinetic terms for the metric.

The matter Lagrangian  $L_{\text{matter}}$  generically will be a functional of a collection of matter fields (denoted as  $\psi$ ) along with  $g_{ab}$  and  $u^a$ . However, following the observational constraints on Lorentz violation in the matter sector, we assume here when studying the neutron star solutions that there is no significant coupling of matter to  $u^a$ . The absence of coupling of  $u^a$  to matter has no theoretical justification in this purely phenomenological approach, and may be regarded as unnatural. However our goal here is just to explore consequences of gravitational Lorentz violation in a phenomenologically viable setting. It remains an open question whether this can emerge as an approximation to a more fundamental underlying theory.

The field equations from varying (1) with respect to  $g^{ab}$ ,  $u^a$  and  $\lambda$  are given by

$$G_{ab} = T_{ab}^{(u)} + 8\pi GT^M_{ab} \quad (4)$$

$$\nabla_a J^a_m - c_4 \dot{u}_a \nabla_m u^a = \lambda u_m, \quad (5)$$

$$g_{ab} u^a u^b = 1, \quad (6)$$

where

$$J^a_m = K^{ab}_{mn} \nabla_b u^n. \quad (7)$$

The aether stress tensor is given by

$$\begin{aligned} T^{(u)}_{ab} = & \nabla_m (J_{(a}^m u_{b)}) - J^m_{(a} u_{b)} - J_{(ab)} u^m \\ & + c_1 [(\nabla_m u_a)(\nabla^m u_b) - (\nabla_a u_m)(\nabla_b u^m)] \\ & + c_4 \dot{u}_a \dot{u}_b \\ & + [u_n (\nabla_m J^{mn}) - c_4 \dot{u}^2] u_a u_b \\ & - \frac{1}{2} L_u g_{ab}, \end{aligned} \quad (8)$$

where  $L_u = -K^{ab}_{mn} \nabla_a u^m \nabla_b u^n$ . The Lagrange multiplier  $\lambda$  has been eliminated from (8) by solving for it via the contraction of the aether field equation (5) with  $u^a$ .

## 2.1 Observational constraints on the parameters $c_i$

In the weak-field, slow-motion limit ae-theory reduces to Newtonian gravity [25], with a value of Newton's constant  $G_N$  related to the parameter  $G$  in the action (1) by

$$G_N = \frac{G}{1 - (c_1 + c_4)/2}. \quad (9)$$

The phenomenology of Einstein-aether theory has been extensively studied over the last few years. Theoretical and observational constraints on the coupling parameters  $c_i$  have been determined from parameterized post-Newtonian analysis [26, 27, 28], stability and linearized energy positivity [29, 30, 31, 32], primordial nucleosynthesis [25], and vacuum Čerenkov radiation [31]. The combined constraints from all of these are reviewed in Ref. [28].

To summarize here, all parameterized post-Newtonian (PPN) parameters except the preferred frame parameters  $\alpha_{1,2}$  agree with those of GR for any choice of the  $c_i$ . Observations impose strong constraints on  $\alpha_1$  ( $\lesssim 10^{-4}$ ) and  $\alpha_2$  ( $\lesssim 4 \times 10^{-7}$ ). These parameters can be set to zero in Einstein-aether theory by imposing two conditions, on the  $c_i$ , which can be solved to determine

$$\begin{aligned} c_2 &= (-2c_1^2 - c_1c_3 + c_3^2)/3c_1 \\ c_4 &= -c_3^2/c_1. \end{aligned} \tag{10}$$

With this choice the gravitational constant appearing in the cosmological Friedman equations agrees with that appearing in the force law between isolated masses, so there is no further nucleosynthesis constraint. The stability, positive energy, and vacuum Čerenkov constraints then impose the inequalities

$$\begin{aligned} 0 &< c_+ < 1 \\ 0 &< c_- < c_+/3(1 - c_+), \end{aligned} \tag{11}$$

where  $c_{\pm} = c_1 \pm c_3$ .

Further constraints have been obtained using radiation damping in binary pulsar systems [33]. An analysis neglecting strong self-gravitating effects found that when (10) hold, just one condition  $\mathcal{A}(c_1, c_3) = 1$  makes the lowest order radiation rate in ae-theory identical to that of GR. This condition is satisfied entirely in the region allowed by (11).<sup>4</sup> However, the neutron star sources are strongly self-gravitating. It turns out [34] that as long as  $c_i \lesssim 0.1$ , the strong field corrections are negligible, but for larger coupling values the precise radiation damping constraints are not yet worked out. They will lead to a modified condition  $\mathcal{A}'(c_1, c_3) = 1$  that will depend on the nature of the compact objects in the binary.

---

<sup>4</sup>In [33], the  $\mathcal{A} = 1$  curve does not fall entirely in the otherwise allowed region, but this is due to an error in the analysis there that has since been corrected [34].

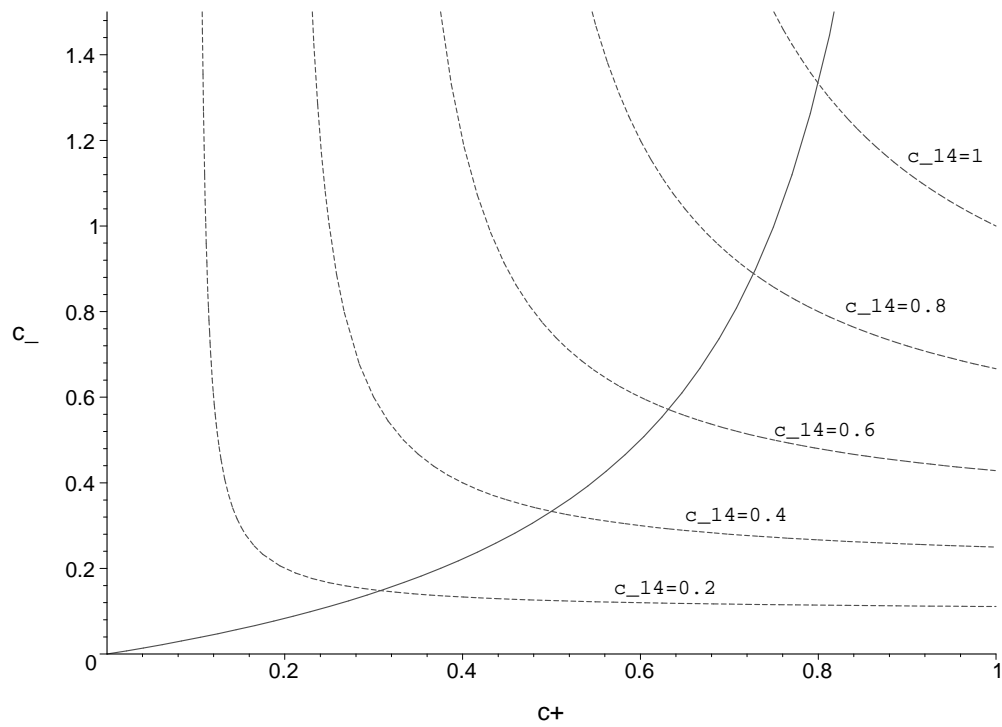


Figure 1: Graphical representation of (11) (solid line) and (12) (dashed lines). The allowed region of the parameter space is below the solid curve, above  $c_- = 0$  and to the left of  $c_+ = 1$ . The radiation damping constraint will restrict to a nearly one-dimensional subset of this region.

Neutron star structure constraints along the lines discussed in the present paper should eventually be able to restrict  $c_{14} = c_1 + c_4$ , which is given by

$$c_{14} = 2c_+c_-/(c_+ + c_-) \quad (12)$$

when the PPN equivalence conditions (10) hold. The only previous constraint on  $c_{14}$  was the requirement that it be less than 2 in order to maintain positivity of Newton's constant (9).

Fig. 1 shows the region in the  $(c_+, c_-)$  parameter space allowed by the above constraints (other than the radiation damping constraint), along with  $c_{14}$  contours. Note that without a constraint on  $c_{14}$ ,  $c_-$  can grow arbitrarily large as  $c_+ \rightarrow 1$ . Any upper bound on  $c_{14}$  will cut off this region however. A  $c_{14}$  contour intersects the right hand boundary ( $c_+ = 1$ ) of the allowed region at  $c_- = c_{14}/(2 - c_{14})$ , and intersects the upper boundary at  $c_- = (4/3)c_{14}/(2 - c_{14})$ .

### 3 Neutron Stars

Time independent spherically symmetric solutions in ae-theory were extensively studied recently in a pair of papers on fluid star [35] and black hole [36] configurations. For black holes, the aether vector has a radial component, but for the case of a star it does not, i.e. it is aligned with the static frame defined by the Killing vector, both inside and outside the star. Thus, unlike in GR, the exterior solution for a star is not the same as for a black hole.

In Ref. [35] the static vacuum exterior solution was found analytically, and numerical integration was employed to find interior stellar solutions for the test case of a constant mass density equation of state. The mass was found by matching the interior to the exterior solutions. Unlike constant density stars in General Relativity (GR), the mass does not increase monotonically with central pressure; rather, there is a maximum mass at a finite central pressure beyond which the stars are unstable. This maximum mass is smaller than in the GR case.

It is adequate for our present purposes to restrict attention to non-rotating stars, since the effect of rotation on the maximum mass, surface redshift, and ISCO is very small for the observationally relevant spins. For example, presuming the fractional change in maximum mass scales with the square of the spin, Tables 4 and 5 in Ref. [37] indicate that even for a one millisecond period the increase of maximum mass is less than 5% in GR.

Barring an unexpected much greater sensitivity to a small spin in ae-theory, the results we find here for non-rotating stars should be quite reliable except for the fastest spinning stars.

### 3.1 Stellar Equations of Structure

The static, spherically symmetric form for the metric and aether can be written in Schwarzschild-like coordinates as

$$ds^2 = e^{A(r)} dt^2 - B(r) dr^2 - r^2 d\Omega^2, \quad (13)$$

$$u = e^{-A(r)/2} \partial_t. \quad (14)$$

Note that since the aether is aligned with the timelike Killing vector it is completely determined by the metric. In particular, the aether is at rest with respect to the static frame at infinity, which means that the star is taken to be at rest with respect to the aether. When comparing theory and observation, it is typically assumed that the background aether frame coincides with that of the cosmological fluid. Any particular star will of course have some proper motion with respect to this frame, so strictly speaking the physically relevant solutions are not of the form (13,14). However, assuming a relative velocity of order  $10^{-3}$ , this discrepancy should not be significant for comparisons of much less precision such as concern us here.

It was shown in [35] that for configurations of the form (13,14) the  $c_2$  and  $c_3$  terms in the action (1) and their variations are zero, and thus they do not contribute to the field equations. Also, the effect of the  $c_4$  term can be absorbed by the replacement  $c_1 \rightarrow c_1 + c_4$ . Hence the only coupling relevant to these solutions is  $c_{14} \equiv c_1 + c_4$ . The fluid stress tensor appearing in the metric field equation (4) is

$$T_{ab}^M = (\rho(r) + P(r)) v_a v_b - P(r) g_{ab} \quad (15)$$

where  $v^a = e^{-A/2} (\partial_t)^a$  is the fluid 4-velocity,  $\rho(r)$  its mass density, and  $P(r)$  its pressure.

The metric field equation and the Bianchi identity together imply that the sum of the aether and fluid energy-momentum tensors is divergenceless. In addition, since the aether does not couple directly to the fluid, its stress tensor is independently divergenceless when its field equation and unit constraint are satisfied. Therefore the fluid stress tensor is also independently divergenceless in any solution. Thus, an appropriate system of equations for the aether plus

fluid case is the (i) metric field equation, (ii) aether field equation, (iii) radial component of  $\nabla^a T_{ab}^M = 0$ , which is the hydrostatic equilibrium equation for the fluid

$$P' + \frac{1}{2}A'(\rho + P) = 0, \quad (16)$$

and (iv) an equation of state  $\rho = \rho(P)$ .

It turns out that the aether field equation (5) has only a  $t$  component, which just determines the Lagrange multiplier  $\lambda$ . The  $tt$ ,  $rr$ , and  $\theta\theta$  components of the metric field equation then imply respectively

$$0 = -1 + B + r\frac{B'}{B} - \nu(8rA' + r^2A'^2 - 2r^2A'\frac{B'}{B} + 4r^2A'') - \rho r^2B \quad (17)$$

$$0 = 1 - B + rA' + \nu r^2A'^2 - Pr^2B \quad (18)$$

$$0 = \frac{1}{4}(2rA' - 2r\frac{B'}{B} + r^2A'^2 - r^2A'\frac{B'}{B} + 2r^2A'') - \nu r^2A'^2 - PB, \quad (19)$$

where the symbol

$$\nu = \frac{c_{14}}{8} \quad (20)$$

is introduced to compactify the notation, and we have adopted units with  $8\pi G = 1$ .

Equation (18) can be used to solve for  $B$ ,

$$B = (1 + r^2P)^{-1}(1 + rA' + \nu r^2A'^2). \quad (21)$$

After substituting this result into (17) and (19),  $A''$  can be eliminated from this pair of equations, yielding an equation involving  $A$ ,  $A'$ ,  $P$ ,  $P'$ , and  $\rho(P)$ . Due to its complexity it does not seem illuminating to display it here. This equation combined with (16) can then be numerically integrated to solve for  $P(r)$  and  $A(r)$  starting with initial values at the origin  $r = 0$ . (It is possible to eliminate  $A'$ , leaving one Tolman-Oppenheimer-Volkoff (TOV) type equation for  $P(r)$ . Since this TOV equation is quite complicated and doesn't aid the numerical integration procedure we will not display it here.)

To numerically integrate outward we find the power series solution to the equations (16) and (17,18,19) in the vicinity of  $r = 0$ , which is a singular point for the equations. In this solution the central value for the pressure  $P(0) = P_0$  is the only free parameter to be specified ( $A(0)$  is arbitrary due to scaling freedom of the  $t$  coordinate, so can just be set to unity). The numerical integration can then be started at a small value of  $r$  using the power series for initial data, and continued to the value  $r = R$ , which is the

surface of the star where the pressure and mass density drop to zero. At this point the values of  $A$  and  $A' > 0$  can be matched to the static vacuum aether solution discussed in [35] and summarized in the next section.

### 3.2 Vacuum solution

In the exterior (21) becomes

$$B = 1 + rA' + \nu r^2 A'^2, \quad (22)$$

and the remaining field equations (17) and (19) can be reduced to the second order ordinary differential equation (ODE)

$$r^2 A'' + 2rA' + r^2 A'^2 + \nu r^3 A'^3 = 0, \quad (23)$$

With the substitution

$$Y = rA', \quad (24)$$

(23) becomes a first order equation for  $Y(r)$  that can be solved, after which (24) can be solved for  $A(Y)$ . In terms of the roots of  $B$ ,

$$Y_{\pm} = (-1 \pm \sqrt{1 - 4\nu}) / (2\nu), \quad (25)$$

the result is

$$B = \nu(Y - Y_-)(Y - Y_+), \quad (26)$$

$$N = e^A = \left( \frac{1 - Y/Y_-}{1 - Y/Y_+} \right)^{\frac{-Y_+}{2+Y_+}}, \quad (27)$$

and

$$\frac{r_{\min}}{r} = \left( \frac{Y}{Y - Y_-} \right) \left( \frac{Y - Y_-}{Y - Y_+} \right)^{\frac{1}{2+Y_+}}, \quad (28)$$

where  $r_{\min}$  is an integration constant. Thus the complete solution is known up to the inversion of the function on the right hand side of (28).

As in GR, the solutions in this family are all asymptotically flat. The limit  $Y \rightarrow 0$  corresponds to spatial infinity, where the limiting form of the solution is

$$B = 1 + Y + \dots \quad (29)$$

$$N = 1 - Y + \dots \quad (30)$$

$$Y = r_g/r + \dots \quad (31)$$

Here  $r_g$  is the gravitational radius, which is related to the gravitational mass  $M$  appearing in the Newtonian potential by

$$r_g = 2G_N M. \quad (32)$$

The relation between  $r_g$  and the minimum radius<sup>5</sup>  $r_{min}$  is given by

$$r_{min}/r_g = (-Y_+)^{-1}(-1 - Y_+)^{(1+Y_+)/(2+Y_+)}. \quad (33)$$

To leading order in  $1/r$  this solution agrees with the Schwarzschild solution of GR. The total gravitational mass  $M$  of the fluid star can be read off from (33) together with (28), using the definition (24),  $Y(R) = RA'(R)$ .

### 3.2.1 Surface redshift

The light emitted from the surface of the neutron star is redshifted as it climbs away to a distant observer. From (13), the surface redshift factor  $z$  is given by

$$z = [N(R)]^{-1/2} - 1, \quad (34)$$

which can be evaluated directly from the numerical solution using (27) and (24).

### 3.2.2 ISCO

The orbits in the metric (13) have conserved energy  $e = N\dot{t}$  and angular momentum  $\ell = r^2\dot{\phi}$ , where  $N = e^A$  and the overdot stands for derivative with respect to proper time. Since the parameter is proper time, the four-velocity has unit norm. This condition can be expressed in the form

$$\dot{r}^2 = V(r) = B^{-1}W, \quad (35)$$

with

$$W = W(r; e, \ell) = N^{-1}(r)e^2 - r^{-2}\ell^2 + 1. \quad (36)$$

The ISCO is determined by the conditions  $V = V' = V'' = 0$ , or equivalently,  $W = W' = W'' = 0$ , where the prime stands for derivative with respect to

---

<sup>5</sup>In the pure vacuum solution, there is a minimal 2-sphere “throat” at  $r = r_{min}$ . In a fluid star solution the radius of the star is always greater than  $r_{min}$ , so there is no throat in the spatial geometry [35].

$r$ . Thus the metric function  $B$  plays no role. These equations determine  $r$ ,  $e$  and  $\ell$  at the ISCO. After some manipulation of the equations we obtain

$$Y_{\text{ISCO}} = \frac{-1 + \sqrt{1 + \nu}}{\nu} \quad (37)$$

With this result, the radius of the ISCO can be found from (28) and (33) given the mass. Expanding in  $\nu = c_{14}/8$  we find (in units with  $G_{\text{N}}M = 1$ )

$$r_{\text{ISCO}} \simeq 6(1 + [\ln(3/2) - 1/6]\nu) \simeq 6(1 + 0.030 c_{14}), \quad (38)$$

dropping  $O(\nu^2)$  terms. This linear approximation is extremely accurate: the relative error grows monotonically from 0 to only about 0.3% over the entire allowed range of  $c_{14}$  from 0 to 2.

The angular frequency of an orbit with respect to time at infinity is given by  $\omega = \dot{\varphi}/\dot{t} = (\ell/e)(N/r^2)$ . The circular orbit condition yields  $N\ell/e = (N'r^3/2)^{1/2} = r(YN/2)^{1/2}$ , so  $\omega = r^{-1}(YN/2)^{1/2}$ . Expanding again in  $\nu$ , the frequency at the ISCO is found (in units with  $G_{\text{N}}M = 1$ ) to be

$$\omega_{\text{ISCO}} \simeq \frac{1}{6\sqrt{6}}(1 + [-2 \ln(3/2) + 1/2]\nu) \simeq \frac{1}{6\sqrt{6}}(1 - 0.039 c_{14}), \quad (39)$$

dropping  $O(\nu^2)$  terms.

Thus, even for the maximum value  $c_{14} = 2$ , the location of the ISCO is only about 6% larger than its value in GR for a star of the same mass, and the orbital frequency is about 8% smaller. Since ae-theory agrees so closely with GR on these quantities, it is unlikely that in the near future any useful constraints can be obtained from their behavior for slowly rotating stars. However, as we discuss in Section 5, for the ISCO of a rapidly rotating black hole the deviations from GR may well be much more pronounced.

## 4 Numerical results

Here we will compare the properties of neutron stars in GR and ae-theory using three hadronic and three quark equations of state (EOS). We label these according to whether they are softer (s), medium (m), or harder (h), by

$$\text{Hs, Hm, Hh} \leftrightarrow \text{A18, A18}\delta v\text{UIX, A18UIX} \quad (40)$$

$$\text{Qs, Qm, Qh} \leftrightarrow (90, 0), (60, 200), (60, 0). \quad (41)$$

The hadronic models are discussed in [38], and the quark models are MIT bag models [39] determined by two parameters  $(B, m_s)$ , with the bag constant  $B$  measured in  $\text{MeV}/\text{fm}^3$  and the strange quark mass  $m_s$  in MeV.

The pressure and mass density data tables for these models [40] were converted from cgs units to geometrized units, i.e. replacing the energy density  $\rho$  and pressure  $p$  by  $G_N\rho/c^4$  and  $G_N p/c^4$  respectively, yielding quantities with dimension inverse length squared. A curve fitting procedure was then used to generate an equation of state function  $\rho(P)$  suitable for the numerical integration. The field equations (17-19) are written in units with  $8\pi G = c = 1$ , so to apply them we first multiply the density and pressure in the above geometrized units by  $8\pi G/G_N = 8\pi(1 - c_{14}/2)$ .

In GR five of the six equations of state have associated  $M$  versus  $P_0$  curves containing a maximum mass extremum and regions of stability and instability. The exception is the softest quark EOS, Qs, which appears to asymptote to its maximum mass value. The GR maximum mass values for the Hm and Hs equations of state we find here ( $2.20M_\odot$  and  $1.67M_\odot$  respectively) agree very well with the results obtained in [38]. The maximum mass value in ae-theory grows smaller and occurs at smaller values of central pressure as  $c_{14}$  is increased. For the Qs EOS extrema begin to develop in the  $M$  versus  $P_0$  curve as  $c_{14}$  approaches 1. Fig. 2 shows a plot of  $M$  vs.  $R$  for the Hm EOS, each point being determined by a value of  $P_0$ , for several values of  $c_{14}$ . As  $P_0$  increases the mass values increase sharply to peaks and then gradually fall off. The region of the curves for small  $P_0$  and larger  $R$  up to the mass maximum describe stable equilibrium configurations. Beyond the maximum the neutron stars are unstable. In ae-theory the minimum radius where the equilibrium configuration is stable decreases as  $c_{14}$  increases.

A plot of the maximum mass values for the six equations of state considered in this paper is shown in Fig. 3. Horizontal lines mark the certain lower bound of  $1.44 M_\odot$  and a benchmark value of  $2.0 M_\odot$ . The dependence of the maximum mass on  $c_{14}$  is very close to linear for the quark models, with the mass changing by roughly 6% as  $c_{14}$  increases from 0 to 1. For the hadronic models it is roughly linear but steeper, decreasing by roughly 15% over the same range of  $c_{14}$ .

## 4.1 Maximum mass constraints

The most straightforward constraint on ae-theory comes from comparing the maximum mass values generated with the six equations of state to observa-

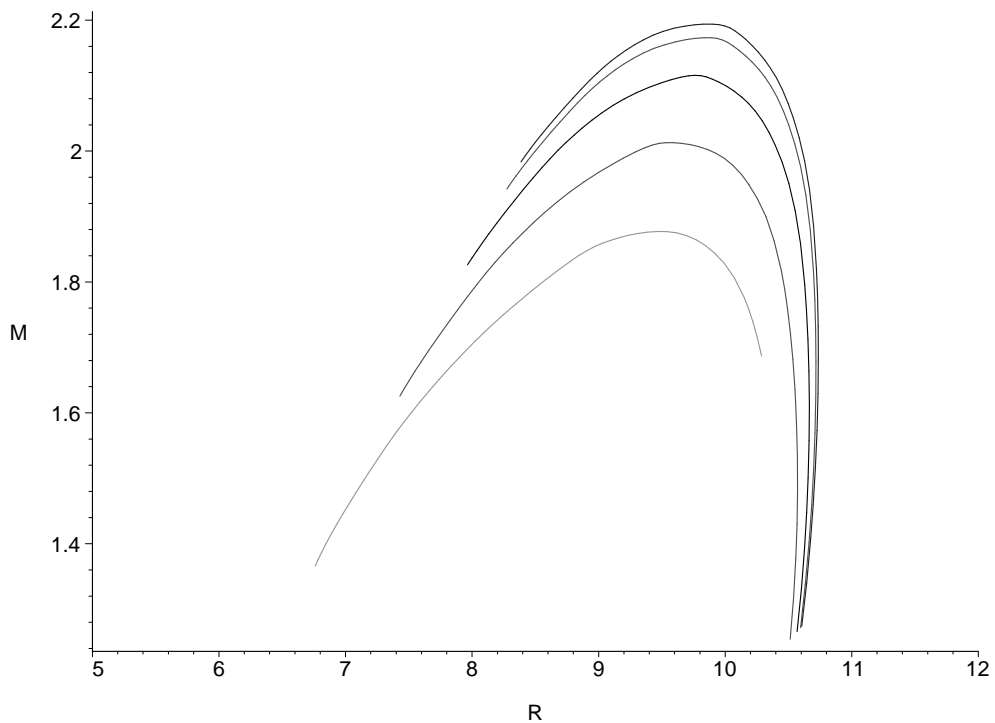


Figure 2: Total mass versus  $R$  for the Hm equation of state for  $P_0$  up to 100 and  $c_{14} = 0, 0.05, 0.2, 0.5, 1$  beginning with the upper (GR) curve. The vertical axis is units of solar masses and the horizontal in km. The GR curve reaches its maximum mass of  $2.20M_{\odot}$  at slightly more than 10 km. As  $c_{14}$  increases to 1 the maximum mass decreases and the value of the radius at the maximum falls to about 9.5 km.

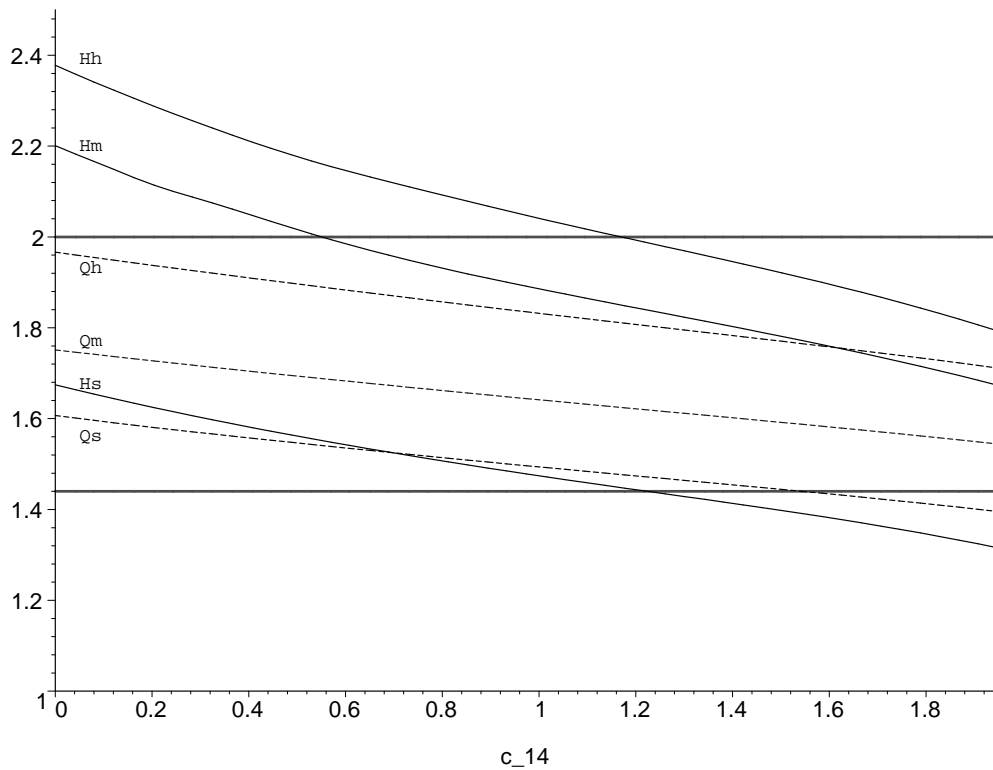


Figure 3: Maximum mass vs.  $c_{14}$  for the six equations of state. The hadronic models are plotted with solid lines, while the quark models are dashed. The thick solid horizontal lines represent the bare minimum constraint of  $1.44 M_{\odot}$  and a possible constraint value of  $2 M_{\odot}$ .

tions of neutron star masses in binary pulsars. These masses are not directly measured, but inferred from the timing data from a binary pulsar system. This data contains information on the Keplerian and post-Keplerian parameters of the system, which depend on the unknown masses  $m_A$  and  $m_B$  of the neutron stars. A determination of the Keplerian and two post-Keplerian parameters, such as the secular rate of periastron advance and the magnitude of the Shapiro delay, result in two curves in a  $(m_A, m_B)$  mass plane. The value of the two masses is the intersection of these curves. Since we are considering the subset of Einstein-aether theories that satisfies the post-Newtonian constraints, any corrections to how the post-Keplerian parameters depend on the pulsar masses would only appear at higher order and is therefore very small. Thus, the masses can be inferred as in GR to a good approximation. If the maximum mass predicted by Einstein-aether theory is smaller than an observed neutron star mass then the theory is ruled out. Currently the largest reliable observed mass value is  $1.44 M_\odot$  from the PSR 1913+16 Hulse-Taylor binary system.

There are, however, suggestions from various data that neutron star masses can be at least  $\sim 2 M_\odot$ . The neutron star in Vela X-1 has an estimated mass of  $1.88 \pm 0.13 M_\odot$  [41], and PSR J0751, a pulsar in a detached low-mass binary, has a reported mass of  $2.1 \pm 0.2 M_\odot$  [42]. Furthermore, there are indications (although not as definitive) for neutron star masses greater than or of order two solar masses in several low-mass X-ray binaries based on the inference of the orbital frequency at the ISCO from their kilohertz quasi-periodic brightness oscillations (QPO's)[43, 44, 45, 46]; for an alternative view, see [47]. At the  $< 700$  Hz spin frequencies of these stars, the dimensionless angular momentum is only 0.1 to 0.3 [37], so this would imply that the ISCO is obtained from a near-Schwarzschild spacetime. Since the ISCO we find in Section 3.2.2 is very close to the GR value, the derived mass should be the same in ae-theory as in GR to a good approximation. As a benchmark, we will consider the limits on  $c_{14}$  that would result from a measured gravitational mass of  $2 M_\odot$ .

Fig. 3 shows that in GR ( $c_{14} = 0$ ) all six equations of state respect the lower bound of  $1.44 M_\odot$  solar masses. For four of the equation of state models the  $1.44 M_\odot$  mass cutoff does not yield any constraint on  $c_{14}$ . For the Hs and Qs EOS there are weak constraints that  $c_{14}$  be less than about 1.2 and 1.5 respectively. The  $2 M_\odot$  constraint is more restrictive. In this case the Hs, Qs, Qm, and Qh EOS are ruled out, while for Hm and Hh  $c_{14}$  must be less than about 0.55 and 1.16 respectively.

As the maximum observed neutron star mass is pushed upwards, and more is learned about the nuclear EOS, the observational upper bound on  $c_{14}$  will come down. If we assume the existence of a non-rotating neutron star of  $2 M_{\odot}$ , then even for the hardest equation of state we have considered we obtain the bound  $c_{14} < 1.16$ .

## 4.2 Surface redshift constraints

There is not yet a definitive detection of an atomic spectral line from the surface of a neutron star. The strongest current case comes from stacked observations of thermonuclear X-ray bursts from EXO 0748–676, from which a surface redshift of 0.35 was inferred [48] based on identification of some absorption-like features as being produced by highly ionized iron. The mass of this star is not certain, but Özel [49] used simplifying assumptions about the constancy of the peak flux of the bursts and radiative transfer to suggest that the mass of this object is probably not less than  $1.8 M_{\odot}$ .

Measurements such as these, once confirmed, can provide a joint constraint on  $c_{14}$  and the equation of state via the dependence of surface redshift on mass in ae-theory. (We have checked that the mass inferred using the method of Ref. [49] differs from the GR value by less than 2% when  $c_{14} = 1$ , so the leading order effect of  $c_{14}$  is only in the relation between radius and mass, equivalently redshift and mass.) Fig. 4 shows a plot of  $z$  versus  $c_{14}$  for  $1.8 M_{\odot}$  stars using the Hm, Hh, and Qh EOS. These are the three hardest equation of state models and have equilibrium configurations at this mass. (As shown in Fig. 3, the other three softest equation of state models do not have equilibrium configurations at this mass.) The surface redshifts increase by roughly 10% as  $c_{14}$  ranges from 0 to 1.

If in the future surface redshifts together with masses can reliably be determined, then tight constraints on the equation of state in GR may be obtained by combining measurements for a collection of stars. It is also possible that single measurements may provide stringent constraints. For example, as revealed in Fig. 4, the proposed surface redshift 0.35 of EXO 0748–676 [48] is compatible with  $1.8 M_{\odot}$  only for the hardest eos (Hh) among those we considered. In general, the parameter  $c_{14}$  could not be constrained without separate knowledge of the equation of state. However, in the example just mentioned one could serendipitously tightly constrain both the equation of state and the value of  $c_{14}$ , since a redshift of 0.35 is the lower limit of all the curves at this mass.

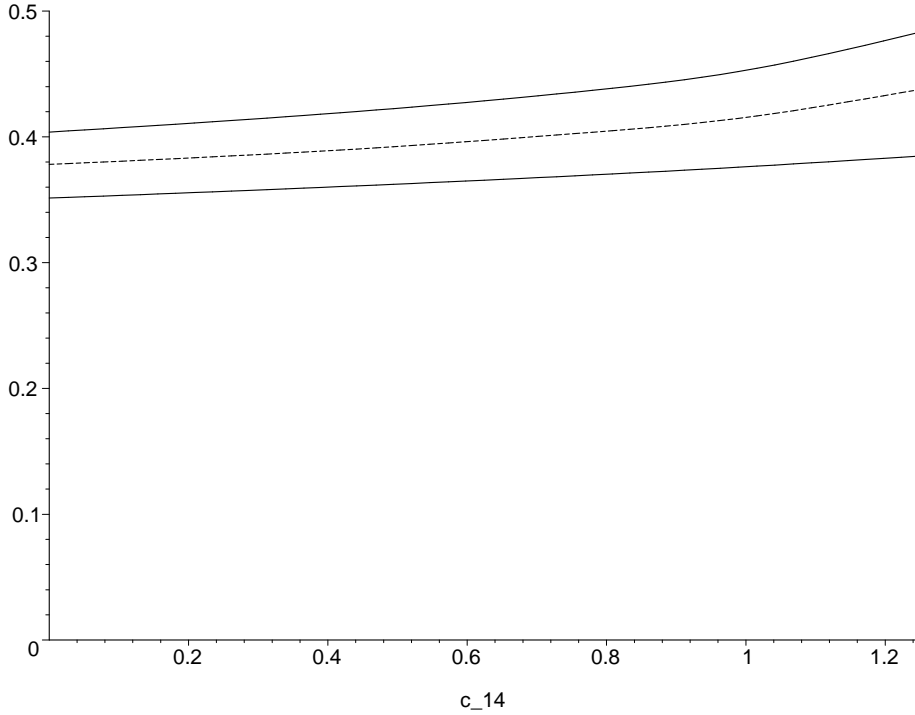


Figure 4: Surface redshift factor  $z$  versus  $c_{14}$  for  $1.8 M_{\odot}$  neutron stars using the hardest equations of state. Hm (solid) is on top, Qh (dashed) is in the middle and Hh (solid) is on the bottom. Note that the GR value of  $z = 0.35$  for the hardest EOS, Hh, is consistent with the proposed surface redshift of 0.35 for EXO 0748–676 [48]. The Hm and Qh lines begin to curve up near  $c_{14} = 1.1-1.2$  because the maximum mass for these equations of state is approaching  $1.8 M_{\odot}$ .

## 5 Discussion

We have found that the structure of non-rotating neutron stars in Einstein-aether theory is fairly close to that in general relativity, but there are quantitative differences. Depending on the equation of state, the maximum masses range from about 6-15% smaller than in GR when the ae-theory parameter  $c_{14}$  is equal to 1. The corresponding surface redshifts are roughly 10% larger than in GR. Measurements of high gravitational masses or precise surface redshifts have the potential to yield strong joint constraints on the equation of state and on deviations from GR. Therefore, as laboratory experiments and other observations narrow down the equation of state of cold matter at several times nuclear density, neutron star observations may be a valuable resource for exploring deviations from general relativity in strong gravity.

We now make some comments about related further work that would be interesting to pursue. First, the neutron star solutions we considered are at rest with respect to the asymptotic aether. Although corrections due to motion with respect to the aether are not significant for the present paper, they are important for the high precision predictions of radiation damping in compact binaries. In particular, the missing ingredient in the analysis of [34] is the value of the “sensitivity” parameter measuring the velocity dependence of the mass. It should be possible to compute this parameter for different masses and different equations of state by determining the velocity perturbations of the solutions found here, or by finding the exact nonlinear solutions with finite velocity.

We considered in this paper only neutron star phenomenology. What is the situation for black holes? It was found in [36] that although different from stellar exteriors, nonrotating black hole solutions in ae-theory are very similar to the Schwarzschild solution of GR. Hence it is not likely that these could lead to significant constraints.

Nevertheless, it is quite conceivable that strong deviations from GR will be found for rapidly rotating black hole solutions. This is suggested by the presence of the ergoregion, in which the inertial frames are strongly dragged. The preferred frame aspects of ae-theory may be conspicuous here, due to larger gradients in the aether field. Also, unlike for the spherically symmetric non-rotating case, the spin-1 degrees of freedom of the aether could be activated in the axially symmetric setting. To explore these issues would require finding numerical solutions describing rotating black holes in Einstein-aether theory.

## Acknowledgments

We are grateful to Sudip Bhattacharyya for kindly providing us with tables characterizing the nuclear equations of state used in our analysis. This work was supported in part by the National Science Foundation under grants PHY-0601800 and AST-0607428.

## References

- [1] M. Kramer et al., “Tests of General Relativity from Timing the Double Pulsar,” *Science* **314**, 97 (2006).
- [2] K. Iwasawa et al., “The variable iron K emission line in MCG-6-30-151996,” *Mon. Not. R. Astron. Soc.* **282**, 1038 (1996).
- [3] A. C. Fabian et al., “A long hard look at MCG-6-30-15 with XMM-Newton,” *Mon. Not. R. Astron. Soc.* **335**, L1 (2002).
- [4] C. S. Reynolds and M. A. Nowak, “Fluorescent iron lines as a probe of astrophysical black hole systems,” *Phys. Rep.* **377**, 389 (2003).
- [5] C. S. Reynolds, L. W. Brenneman and D. Garofalo, “Black Hole Spin in AGN and GBHCs,” *Astrophys. Space Sci.* **300**, 71 (2005).
- [6] L. W. Brenneman and C. S. Reynolds, “Constraining Black Hole Spin via X-Ray Spectroscopy,” *Astrophys. J.* **652**, 1028 (2006).
- [7] N. White, “The Constellation-X Mission,” High Resolution X-ray Spectroscopy: towards XEUS and Con-X, Proceedings of the international workshop held at the Mullard Space Science Laboratory of University College London, Holmbury St Mary, Dorking, Surrey, UK, March 27 - 28, 2006, Ed. G. Branduardi-Raymont, E41 (2006) <http://www.mssl.ucl.ac.uk/~gbr/workshop2/>.
- [8] B. C. Barish, “The Laser Interferometer Gravitational-Wave Observatory LIGO,” *Adv. Space Res.* **25**, 1165 (2000).
- [9] F. Fidecaro et al., “The Virgo Interferometer for Gravitational Wave Detection,” in *Proc. 12th Italian Conf. on General Relativity and Gravitational Physics*, ed. M. Bassan, V. Ferrari, M. Francaviglia, F. Fucito and I. Modena (Singapore: World Scientific), 163 (1997).

- [10] R. Schilling, “The GEO600 Ground-Based Interferometer for the Detection of Gravitational Waves,” in AIP Conf. Proc. 456, Laser Interferometer Space Antenna, Second International LISA Symp., ed. W. M. Folkner (New York: AIP), 217 (1998).
- [11] M. Ando et al., “Current status of TAMA,” *Class. Quant. Grav.* **19**, 1409 (2002).
- [12] K. Danzmann, “LISA Mission Overview,” *Adv. Space Res.* **25**, 1129 (2000).
- [13] A. Salmona, *Phys. Rev. D* **154** 1218 (1967); W. Hillebrant and H. Heintzmann, *Gen. Relativ. Gravitation* **5** 663 (1974)
- [14] T. Damour and G. Esposito-Farese, “Nonperturbative strong field effects in tensor - scalar theories of gravitation,” *Phys. Rev. Lett.* **70**, 2220 (1993).
- [15] S. DeDeo and D. Psaltis, “Towards New Tests of Strong-field Gravity with Measurements of Surface Atomic Line Redshifts from Neutron Stars,” *Phys. Rev. Lett.* **90**, 141101 (2003) [arXiv:astro-ph/0302095].
- [16] M. A. Clayton and J. W. Moffat, “Scalar-Tensor Gravity Theory For Dynamical Light Velocity,” *Phys. Lett. B* **477**, 269 (2000) [arXiv:gr-qc/9910112].
- [17] T. Jacobson and D. Mattingly, “Gravity with a dynamical preferred frame,” *Phys. Rev. D* **64**, 024028 (2001) [arXiv:gr-qc/0007031].
- [18] N. Arkani-Hamed, H. C. Cheng, M. A. Luty and S. Mukohyama, “Ghost condensation and a consistent infrared modification of gravity,” *JHEP* **0405**, 074 (2004) [arXiv:hep-th/0312099].
- [19] B. M. Gripaios, “Modified gravity via spontaneous symmetry breaking,” *JHEP* **0410**, 069 (2004) [arXiv:hep-th/0408127].
- [20] R. Bluhm and V. A. Kostelecky, “Spontaneous Lorentz violation, Nambu-Goldstone modes, and gravity,” *Phys. Rev. D* **71**, 065008 (2005) [arXiv:hep-th/0412320].

- [21] C. Heinicke, P. Baekler and F. W. Hehl, “Einstein-aether theory, violation of Lorentz invariance, and metric-affine gravity,” *Phys. Rev. D* **72**, 025012 (2005) [arXiv:gr-qc/0504005].
- [22] V. A. Rubakov, “Phantom without UV pathology,” *Theor. Math. Phys.* **149**, 1651 (2006) [*Teor. Mat. Fiz.* **149**, 409 (2006)] [arXiv:hep-th/0604153].
- [23] H. C. Cheng, M. A. Luty, S. Mukohyama and J. Thaler, “Spontaneous Lorentz breaking at high energies,” *JHEP* **0605**, 076 (2006) [arXiv:hep-th/0603010].
- [24] C. Eling, T. Jacobson and D. Mattingly, “Einstein-aether theory,” in *Deserfest*, eds. J. Liu, M. J. Duff, K. Stelle, and R. P. Woodard (World Scientific, 2006) arXiv:gr-qc/0410001.
- [25] S. M. Carroll and E. A. Lim, “Lorentz-violating vector fields slow the universe down,” *Phys. Rev. D* **70**, 123525 (2004) [arXiv:hep-th/0407149].
- [26] C. Eling and T. Jacobson, “Static post-Newtonian equivalence of GR and gravity with a dynamical preferred frame,” *Phys. Rev. D* **69**, 064005 (2004) [arXiv:gr-qc/0310044].
- [27] M. L. Graesser, A. Jenkins and M. B. Wise, “Spontaneous Lorentz violation and the long-range gravitational preferred-frame effect,” *Phys. Lett. B* **613**, 5 (2005) [arXiv:hep-th/0501223].
- [28] B. Z. Foster and T. Jacobson, “Post-Newtonian parameters and constraints on Einstein-aether theory,” *Phys. Rev. D* **73**, 064015 (2006) [arXiv:gr-qc/0509083].
- [29] T. Jacobson and D. Mattingly, “Einstein–Aether waves,” *Phys. Rev. D* **70**, 024003 (2004) [arXiv:gr-qc/0402005].
- [30] E. A. Lim, “Can We See Lorentz-Violating Vector Fields in the CMB?,” *Phys. Rev. D* **71**, 063504 (2005) [arXiv:astro-ph/0407437].
- [31] J. W. Elliott, G. D. Moore and H. Stoica, “Constraining the new aether: Gravitational Cherenkov radiation,” *JHEP* **0508**, 066 (2005) [arXiv:hep-ph/0505211].

- [32] C. Eling, “Energy in the Einstein-aether theory,” *Phys. Rev. D* **73**, 084026 (2006) [arXiv:gr-qc/0507059].
- [33] B. Z. Foster, “Radiation damping in Einstein-aether theory,” *Phys. Rev. D* **73**, 104012 (2006) [arXiv:gr-qc/0602004].
- [34] B. Z. Foster, “Strong field effects on binary systems in Einstein-aether theory,” arXiv:0706.0704 [gr-qc].
- [35] C. Eling and T. Jacobson, “Spherical Solutions in Einstein–Aether Theory: Static Aether and Stars,” *Class. Quant. Grav.* **23**, 5625 (2006) [arXiv:gr-qc/0603058].
- [36] C. Eling and T. Jacobson, “Black holes in Einstein-aether theory,” *Class. Quant. Grav.* **23**, 5643 (2006) [arXiv:gr-qc/0604088].
- [37] G. B. Cook, S. L. Shapiro and S. A. Teukolsky, “Rapidly rotating neutron stars in general relativity: Realistic equations of state,” *Astrophys. J.* **424**, 823 (1994).
- [38] A. Akmal, V. R. Pandharipande and D. G. Ravenhall, “The equation of state for nucleon matter and neutron star structure,” *Phys. Rev. C* **58**, 1804 (1998) [arXiv:nucl-th/9804027].
- [39] E. Farhi and R. L. Jaffe, “Strange Matter,” *Phys. Rev. D* **30**, 2379 (1984).
- [40] Sudip Bhattacharyya, private communication.
- [41] H. Quaintrell et al., “The mass of the neutron star in Vela X-1 and tidally induced non-radial oscillations in GP Vel,” *Astron. Astrophys.* **401**, 313 (2003).
- [42] D. J. Nice et al., “A  $2.1 M_{\odot}$  Pulsar Measured by Relativistic Orbital Decay,” *Astrophys. J.* **634**, 1242 (2005).
- [43] D. Barret, J.-F. Olive and M. C. Miller, “Drop of coherence of the lower kilo-Hz QPO in neutron stars: Is there a link with the innermost stable circular orbit?,” *Astron. Nachr.* **326**, 808 (2005).

- [44] D. Barret, J.-F. Olive and M. C. Miller, “An abrupt drop in the coherence of the lower kHz quasi-periodic oscillations in 4U 1636-536,” *Mon. Not. R. Astron. Soc.* **361**, 855 (2005).
- [45] D. Barret, J.-F. Olive and M. C. Miller, “The coherence of kilohertz quasi-periodic oscillations in the X-rays from accreting neutron stars,” *Mon. Not. R. Astron. Soc.* **370**, 1140 (2006).
- [46] D. Barret, J.-F. Olive and M. C. Miller, “Supporting evidence for the signature of the innermost stable circular orbit in Rossi X-ray data from 4U 1636-536,” *Mon. Not. R. Astron. Soc.* **376**, 1139 (2007).
- [47] M. Méndez, “On the maximum amplitude and coherence of the kilohertz quasi-periodic oscillations in low-mass X-ray binaries,” *Mon. Not. R. Astron. Soc.* **371**, 1925 (2006).
- [48] J. Cottam, F. Paerels and M. Méndez, “Gravitationally redshifted absorption lines in the X-ray burst spectra of a neutron star,” *Nature (London)* **420**, 51 (2002).
- [49] F. Özel, “Soft equations of state for neutron-star matter ruled out by EXO 0748-676,” *Nature (London)* **441**, 1115 (2006).